Temperature characterisation of spectroscopic InGaP X-ray photodiodes

Article (Accepted Version)

Temperature characterisation of spectroscopic InGaP X-ray photodiodes

S. Butera[1,*)], G. Lioliou[1], A. B. Krysa[2], A. M. Barnett[1]

[1]Space Research Group, School of Engineering and Informatics, University of Sussex, Brighton, BN1 9QT, UK.

[2]EPSRC National Epitaxy Facility, University of Sheffield, Mappin Street, Sheffield, S1 3JD, UK.

Email: S.Butera@sussex.ac.uk (S. Butera)

Tel.: +441273872568

Abstract. In this paper for the first time, an InGaP photodiode was used in a high temperature tolerant X-ray spectrometer. The use of InGaP in X-ray spectrometers shows a significant advance within this field allowing operation up to 100 °C. Such results are particularly important since GaP and InP (the InGaP binary parent compounds) are not spectroscopic even at room temperature. The best energy resolution (smallest FWHM) at 5.9 keV for the InGaP spectrometer was 1.27 keV at 100 °C and 770 eV at 20 °C, when the detector was reverse biased at 5 V. The observed FWHM were higher than the expected statistically limited energy resolutions indicating that other sources of noise contributed to the FWHM broadening. The spectrometer's Si preamplifier electronics was the limiting factor for the FWHM rather than the InGaP photodiode itself. The InGaP electron-hole pair creation energy (ε_{InGaP}) was experimentally measured across the temperature range 100 °C to 20 °C. ε_{InGaP} was 4.94 eV ± 0.06 eV at 20 °C.

Keywords: InGaP; X-ray spectroscopy; electron-hole pair creation energy; semiconductor.

1. INTRODUCTION

* Author to whom correspondence should be addressed.

High-resolution X-ray astronomy and X-ray fluorescence spectroscopy [1] have been made possible because of the use of photon counting X-ray spectrometers. The ability to determine the energy of individual X-ray photons and the number of the detected X-ray photons at a particular energy can be essential in space missions. These attributes are particularly useful to study planetary surfaces, magnetospheres, and solar physics, as well as for terrestrial applications such as industrial monitoring and non-destructive testing. The use of wide bandgap materials in such spectrometers is attractive because such materials can have low thermally generated leakage currents; as such they can operate at high temperatures without cooling systems thus resulting in more compact, lower mass, and lower power instrumentation.

High energy resolution and temperature tolerant photon counting X-ray spectrometers have been reported using various wide bandgap semiconductors detectors coupled to low-noise preamplifiers electronics [2, 3, 4, 5]. Lioliou et al. [2] reported a GaAs diode with energy resolution (Full Width at Half Maximum, FWHM) at 5.9 keV of 840 eV at 60 °C. Barnett et al. [3] demonstrated an $Al_{0.8}Ga_{0.2}As$ detector with energy resolution at 5.9 keV of 2.2 keV at 90 °C. In both cases the Si preamplifier electronics were also operated uncooled at the same temperature as the compound semiconductor photodetector. A SiC X-ray spectrometer with an energy resolution at 5.9 keV of 233 eV at 100 °C has also been developed by Bertuccio et al. [4]. Recently, another wide bandgap semiconductor, $Al_{0.52}In_{0.48}P$, has shown exceptional promise as a newly emerging material for photon counting X-ray spectroscopy. Butera et al. [5] reported an $Al_{0.52}In_{0.48}P$ detector spectrometer with an energy resolution at 5.9 keV of 1.57 keV at 100 °C and 0.90 keV at 20 °C. The spectroscopic performance of CdTe and CdZnTe detectors has also been investigated at high temperature. Squillante et al. [6] reported a CdTe spectrometer with an energy resolution at 122 keV of 53 keV at 92 °C. Egarievwe et al. [7] developed a CdZnTe spectrometer with an energy resolution at 32 keV of 9.4 keV at 70 °C. CdTe and CdZnTe detectors have been widely developed for room temperature X-ray spectroscopy. For example, Zappettini et al. [8] demonstrated CdZnTe detectors with an energy resolution at 59.5 keV of 2.5 keV using low-noise application specific integrated circuit (ASIC) readout electronics. Abbene et al. [9] reported a CdZnTe structure showing energy resolutions of 3.8% (2.26 keV) and 3.2% (3.91 keV) at 59.5 keV and 122.1 keV, respectively, at low count rate. Recently an $In_{0.5}Ga_{0.5}P$ X-ray photodiode was also demonstrated to be spectroscopic at room

temperature when coupled to a low noise charge sensitive preamplifier [10]. This was particularly surprising given that its parent materials InP and GaP had been previously found to be non-spectroscopic [11, 12, 13, 14]. The use of $In_{0.5}Ga_{0.5}P$ is important because it has large X-ray and γ-ray attenuation coefficients leading to high quantum detection efficiencies per unit thickness [15, 16].

In this paper, for the first time, an $In_{0.5}Ga_{0.5}P$ p^+-i-n^+ mesa photodiode was coupled to a custom-made low-noise charge-sensitive preamplifier and investigated for its performance at high temperature (from 100 °C to 20 °C). The material's electron-hole pair creation energy was also determined. The performance of the spectrometer was analysed under the illumination of a 192 MBq ^{55}Fe radioisotope X-ray source over the temperature range using different shaping times and applied biases. At 100 °C, the best energy resolution at 5.9 keV was 1.27 keV, which improved to 770 eV at 20 °C. The different noise contributors to these determined energy resolutions were computed and are discussed in detail. The electron-hole pair creation energy, ε_{InGaP}, was measured using a dedicated experiment. It was found that ε_{InGaP} = 4.94 eV ± 0.06 eV at 20 °C. ε_{InGaP} is the average energy consumed in the generation of an electron-hole pair during the creation of a charge cloud of electron-hole pairs upon absorption of an X-ray photon within $In_{0.5}Ga_{0.5}P$.

2. EXPERIMENTAL

2.1 STRUCTURE DESIGN

An $In_{0.5}Ga_{0.5}P$ p^+-i-n^+ epilayer was grown on a heavily doped n^+ GaAs substrate by low-pressure (150 Torr) metalorganic vapour phase epitaxy using trimethylgallium, trimethylindium, arsine, and phosphine as precursors, and hydrogen as a carrier gas. Disilane and dimethylzinc:triethylamine were used for n- and p-doping, respectively. The epitaxial surface of the substrate had an orientation of (100) with a miscut angle of 10° towards the GaAs <111> plane terminating with Ga atoms. The unintentionally doped i layer (thickness of 5 μm) was between a top p^+ layer (thickness of 0.2 μm; doping concentration of 2×10^{18} cm^{-3}) and a bottom n^+ layer (thickness of 0.1 μm; doping concentration of 2×10^{18} cm^{-3}). It has to be noted that the thickness of the p^+ and n^+ layers were as thin as possible such to decrease the absorption in these layers. The thicknesses for the p^+ layer (0.2 μm) and n^+ layer (0.1 μm) were chosen based on

our own experience of growth of high quality $In_{0.5}Ga_{0.5}P$. The thickness of the i layer, instead, was thick to increase the absorption, and consequently the quantum efficiency, in this layer. It has to be highlighted that the $In_{0.5}Ga_{0.5}P$ device is the thickest i layer $In_{0.5}Ga_{0.5}P$ photodiode so far reported; i layers thicker than 5 μm may be produced in the future. On top of the $In_{0.5}Ga_{0.5}P$ p^+-i-n^+ epilayer, a thin p^+ GaAs layer (thickness of 0.01 μm; doping concentration of 1×10^{19} cm^{-3}) was grown to help achieve a good top Ohmic contact. n type GaAs, n type $In_{0.5}Ga_{0.5}P$ and unintentionally doped $In_{0.5}Ga_{0.5}P$ were grown at a temperature of 700 °C, and the subsequent p-doped layers were grown at 660 °C. At room temperature, the grown $In_{0.5}Ga_{0.5}P$ had a photoluminescence peak energy of 1.89 eV. This energy is in good agreement with the bandgap of the material with a suppressed spontaneous long-range ordering in the group III sublattice [17]. The Ohmic contact on top of the p^+ GaAs layer was formed from Ti (thickness of 20 nm) and Au (thickness of 200 nm). The Ohmic rear contact, deposited onto the rear of the n^+ GaAs substrate, was formed from InGe (thickness of 20 nm) and Au (thickness of 200 nm). The $In_{0.5}Ga_{0.5}P$ photodiode was not passivated. Chemical wet etching techniques (1:1:1 $K_2Cr_2O_7$:HBr:CH_3COOH solution followed by a 10 s finishing etch in 1:8:80 H_2SO_4:H_2O_2:H_2O solution) were used to fabricate the 200 μm diameter $In_{0.5}Ga_{0.5}P$ mesa device used in the study. The device layers, their relative thicknesses and materials are summarised in TABLE 1.

TABLE 1. Layer details of the $In_{0.5}Ga_{0.5}P$ photodiode.

Layer	**Material**	**Thickness (μm)**	**Dopant**	**Dopant Type**	**Doping density (cm^{-3})**
1	Ti	0.02			
2	Au	0.2			
3	GaAs	0.01	Zn	p^+	1×10^{19}
4	$In_{0.5}Ga_{0.5}P$	0.2	Zn	p^+	2×10^{18}
5	$In_{0.5}Ga_{0.5}P$	5	undoped		$< 5 \times 10^{16}$
6	$In_{0.5}Ga_{0.5}P$	0.1	Si	n^+	2×10^{18}
7	GaAs buffer	0.3	Si	n^+	2×10^{18}
8	Substrate n^+ GaAs	350	Si	n^+	2×10^{18}
9	InGe	0.02			
10	Au	0.2			

A 192 MBq ^{55}Fe radioisotope X-ray source (Mn Kα = 5.9 keV, Mn Kβ = 6.49 keV) was positioned 5 mm away from the top surface of the 200 μm diameter $In_{0.5}Ga_{0.5}P$ mesa photodiode such as to study the detector performances under illumination.

The $In_{0.5}Ga_{0.5}P$ X-ray quantum efficiencies (*QE*) through the device's optical window (region not covered by contacts) were calculated using the Beer-Lambert law and assuming complete charge collection in the p and i layers. Figure 1 shows the $In_{0.5}Ga_{0.5}P$ X-ray quantum efficiencies as a function of photon energy up to 10 keV.

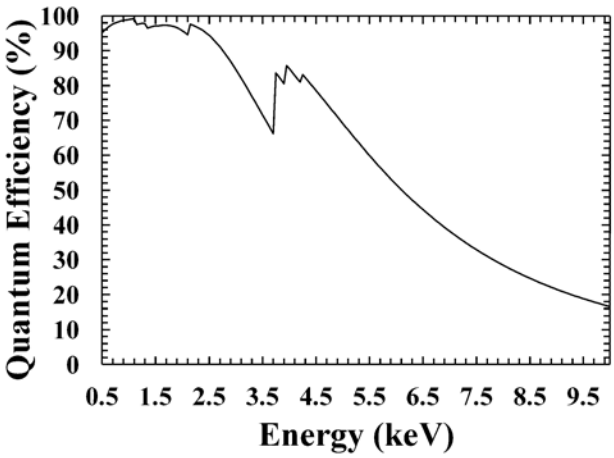

Figure 1. Calculated $In_{0.5}Ga_{0.5}P$ X-ray quantum efficiencies as a function of photon energy.

X-ray quantum efficiencies (*QE*) of 53% at 5.9 keV and 44% at 6.49 keV were computed for the structure. TABLE 2 shows the attenuation coefficients at 5.9 keV and 6.49 keV for $In_{0.5}Ga_{0.5}P$ as well as other different materials. The attenuation coefficients for binary and ternary compounds were estimated from the attenuation coefficients of their single elements, properly weighted [15, 16].

TABLE 2. Attenuation coefficients at 5.9 keV and 6.49 keV for different materials.

Material	**Attenuation coefficient at 5.9 keV (cm^{-1})**	**Attenuation coefficient at 6.49 keV (cm^{-1})**
$In_{0.5}Ga_{0.5}P$	1464	1130
$Al_{0.52}In_{0.48}P$	1301	1004
GaAs	837	642
$Al_{0.8}Ga_{0.2}As$	788	604
Si	346	263

QE at 5.9 keV greater than 90% may be obtained by increasing the $In_{0.5}Ga_{0.5}P$ i layer thickness to 30 µm; this i layer thickness may be achieved in future $In_{0.5}Ga_{0.5}P$ structures as consequence of advances in growth and fabrication technologies. Because of the higher linear attenuation coefficients of $In_{0.5}Ga_{0.5}P$ with respect to SiC, the

quantum efficiency of the 5 μm $In_{0.5}Ga_{0.5}P$ device at high X-ray photon energies (> 48 keV) are expected to be higher than those of a 300 μm SiC detector at the same energies.

2.2 CHARACTERIZATION SETUP

The $In_{0.5}Ga_{0.5}P$ device was installed inside a TAS Micro MT climatic cabinet for temperature control. The temperature was initially set to 100 °C and decreased to 20 °C, in steps of 20 °C. Before taking any measurements at each temperature, the device was left for 30 minutes to ensure stabilisation.

The $In_{0.5}Ga_{0.5}P$ leakage current as a function of reverse bias was measured using a Keithley 6487 picoammeter/voltage source. The uncertainty associated with individual current readings was 0.3% of their values plus 400 fA, while the uncertainty associated with applied biases was 0.1% of their values plus 1 mV [18]. The $In_{0.5}Ga_{0.5}P$ capacitance as a function of reverse bias was measured using an HP 4275A Multi Frequency LCR meter. The uncertainty associated with each capacitance reading was 0.12% [19], while the uncertainty associated with applied biases was 0.1% of their values plus 1 mV [18]. The test signal was sinusoidal with a 50 mV rms magnitude and 1 MHz frequency. In both leakage current and capacitance measurements, the reverse bias increased from 0 V to 15 V (in 1 V increments).

X-ray spectra were obtained using the ^{55}Fe radioisotope X-ray source to illuminate the 200 μm diameter $In_{0.5}Ga_{0.5}P$ device at temperatures from 100 °C to 20 °C. The experimental setup utilised a custom-made charge-sensitive preamplifier of feedback resistorless design, similar to that reported in ref. [20]. The preamplifier was operated at the same temperature as the photodiode. The signal from the preamplifier was shaped by an Ortec 572a shaping amplifier, and digitized by a multichannel analyser (Ortec Easy-MCA-8K). Spectra were accumulated and analysed at shaping times of 0.5 μs, 1 μs, 2 μs, 3 μs, 6 μs, and 10 μs. The $In_{0.5}Ga_{0.5}P$ device was reverse biased at 0 V, 5 V, 10 V, and 15 V, in each case. The live time for each spectrum was 200 s.

All the experiments were performed in dry nitrogen atmosphere (relative humidity <5%) as a precautionary measure to eliminate any formation of water vapor at high temperatures and water condensation at low temperatures inside the chamber.

3. RESULTS

3.1 Current and capacitance measurements

The measured leakage currents of the packaged device at 100 °C and 80 °C are shown in Figure 2; leakage currents at temperatures below 80 °C are not reported because they were below the picoammeter's noise floor. Measurements of the leakage current as a function of the reverse bias of the system when the diode was not connected showed that the system was contributing to the measured leakage current. At 100 °C and at 80 °C, the packaged device (defined as the semiconductor and system combined) had leakage currents of 1.5 pA and 0.5 pA, respectively, at a reverse bias of 10 V. At the same temperatures and reverse bias condition, the system (with no diode connected) had leakage currents of 1.1 pA and 0.2 pA, respectively. When the reverse bias was increased to 15 V in each case, the leakage currents measured for the packaged device and the system became indistinguishable at both temperatures. Considering the uncertainties associated with the leakage current measurements, the leakage current from the diode itself can be considered negligible compared with the other leakage currents.

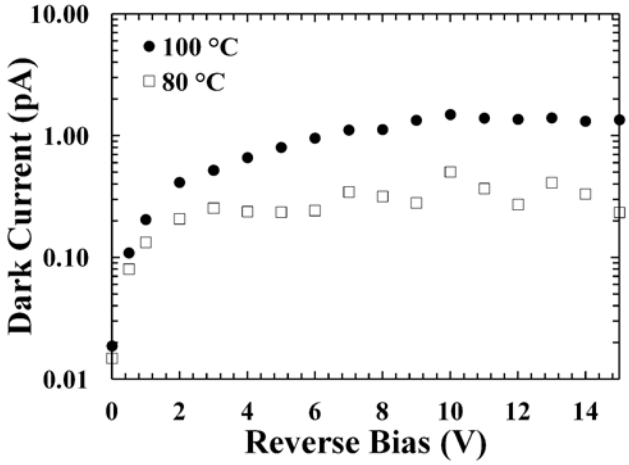

Figure 2. Leakage current of the packaged $In_{0.5}Ga_{0.5}P$ detector (i.e. from both the semiconductor junction and the package) as a function of applied reverse bias at 100 °C (filled circles) and 80 °C (empty squares).

At different temperatures, the capacitance of the packaged $In_{0.5}Ga_{0.5}P$ detector as a function of reverse bias was measured. The capacitance of an empty package of the same type was also measured at different temperatures and subtracted from the

measured capacitance of the packaged $In_{0.5}Ga_{0.5}P$ photodiode. At each temperature, the capacitances were measured multiple times; the mean and its relative root mean squared (RMS) error were considered. The capacitances of the empty package were measured to be 1.27 pF ± 0.02 pF and 1.132 pF ± 0.003 pF at 100 °C and 80 °C, respectively. The uncertainties reflect not only the uncertainty in one measurements, but also the variation in measured value upon repetition; greater variation was seen at 100 °C than at 80 °C. In the temperature range studied, the capacitance of the $In_{0.5}Ga_{0.5}P$ detector itself (C) was found to be temperature invariant. $1/C^2$ as a function of reverse bias at 100 °C and at 80 °C is shown in Figure 3, similar results were found at temperatures ≤ 60 °C. A dependence between $1/C^2$ and the reverse bias was found at reverse biases below 3 V; $1/C^2$ was constant at reverse biases higher than 3 V.

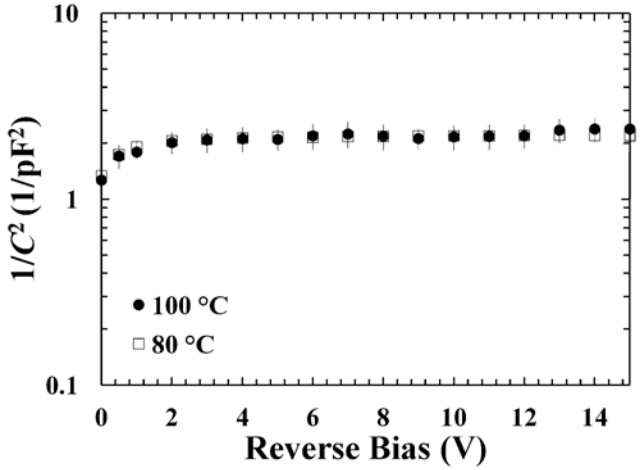

Figure 3. $1/C^2$ as a function of applied reverse bias. The temperatures analysed were 100 °C (filled circles) and 80 °C (empty squares).

3.2 X-ray spectroscopy and noise analysis

X-ray spectra were obtained using the ^{55}Fe radioisotope X-ray source. Although temperatures above 100 °C can be achieved by the TAS Micro MT climatic cabinet, temperatures higher than 100 °C were not studied because of limitations in the working temperature range of the spectrometer's electrical cables. At 100 °C, the diode was stable throughout the spectrum acquisition time. The diode did not degrade after being used at such temperatures. Moreover, polarization phenomena were not observed in the detector at any of the temperatures or biases studied.

An improvement in energy resolution (as quantified by the FWHM at 5.9 keV) was observed when increasing the applied reverse bias from 0 V to 5 V. This result can be explained considering the reduction in capacitance of the detector and possibly improved charge collection. No further change in FWHM was observed when operating the detector at reverse biases > 5 V. The latter behaviour can be explained considering that the $In_{0.5}Ga_{0.5}P$ photodiode is fully depleted above 5 V.

The optimum shaping time (i.e. that which produced the smallest FWHM) varied with temperature, as shown in Figure 4. The FWHM decreased at lower temperatures because of the lower leakage currents of the $In_{0.5}Ga_{0.5}P$ photodiode and Si JFET at such temperatures. The spectra with the best energy resolution (smallest FWHM) at 100 °C and 20 °C with the photodiode reverse biased at 5 V are presented in Figure 5. The observed ^{55}Fe photopeaks were the combination of the characteristic Mn Kα (5.9 keV) and Mn Kβ (6.49 keV) lines of the ^{55}Fe radioisotope X-ray source. To determine the FWHM of the 5.9 keV peaks in Figures 4 and 5, Gaussian fitting was performed on the photopeaks: the Mn Kα and Mn Kβ peaks were deconvolved from detected combined photopeak. The fitting took into account the relative X-ray emission rates of the ^{55}Fe radioisotope X-ray source at 5.9 keV and 6.49 keV in the appropriate ratio [21] as well as the relative efficiency of the detector at these X-ray energies.

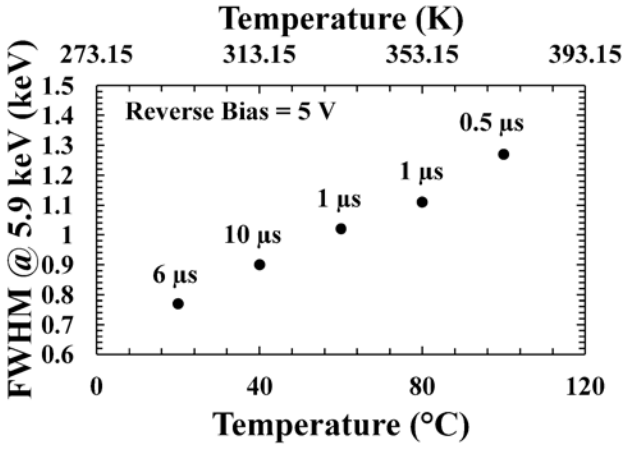

Figure 4. The smallest observed FWHM of the 5.9 keV peak as a function of temperature at the optimum shaping time, when the $In_{0.5}Ga_{0.5}P$ detector was reverse biased at 5 V.

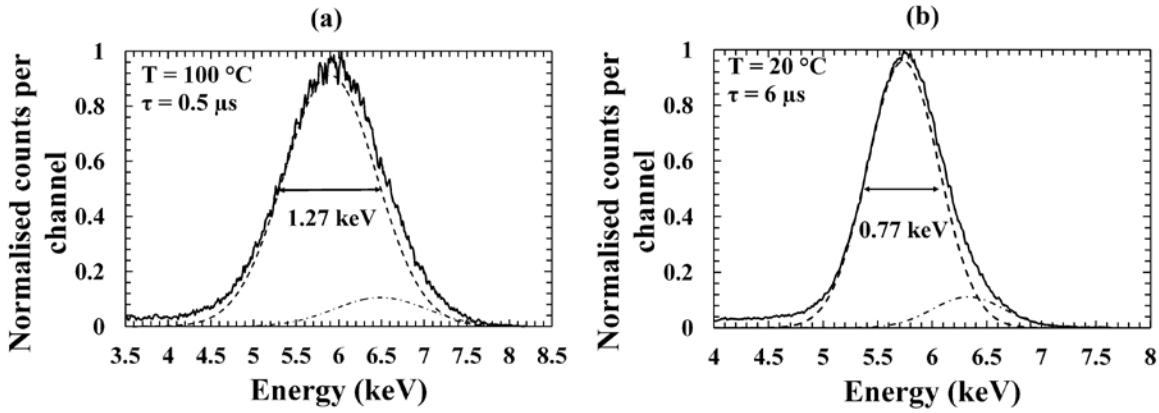

Figure 5. Best energy resolution ^{55}Fe X-ray spectra collected at 100 °C (a) and at 20 °C (b) with the $In_{0.5}Ga_{0.5}P$ photodiode reversed bias at 5 V. Also shown in each spectrum are the deconvolved Mn Kα (dashed line) and Mn Kβ (dashed-dot line) peaks.

The FWHM of the 5.9 keV peak as a function of shaping time at 100 °C and 20 °C, with the photodiode reverse biased at 5 V, are presented in Figure 6.

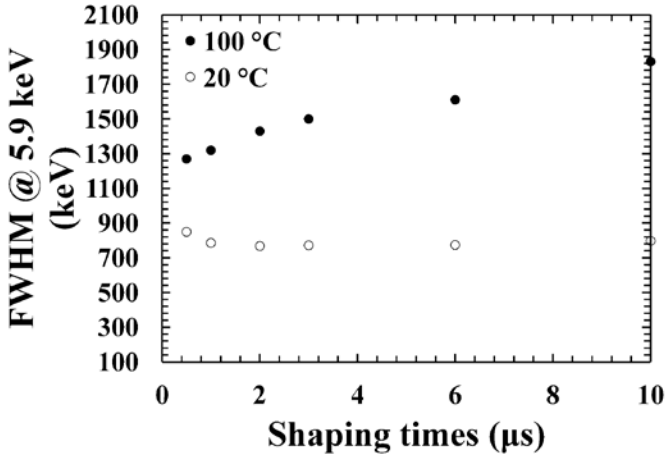

Figure 6. FWHM of the 5.9 keV peak as a function of shaping time at 100 °C (filled circles) and 20 °C (empty circles), when the $In_{0.5}Ga_{0.5}P$ detector was reverse biased at 5 V.

The energy resolution (FWHM) of a non-avalanche X-ray photodiode spectrometer is degraded by the Fano noise, the charge trapping noise, and the electronic noise [22, 23]. The Fano noise is due to the statistical nature of the ionisation process; it is calculated and explained in section "C. Fano-limited energy resolution and electron-hole pair creation energy". At each temperature studied, the observed FWHM was greater than the expected Fano limited energy resolution, indicating that noise sources other than the statistical charge creation process were significant. In a photodiode X-ray spectrometer, the electronic noise is caused by 5 different components: parallel white

noise, series white noise, induced gate current noise, 1/*f* noise, and dielectric noise [22, 23]. The leakage currents of the detector and the Si input JFET of the preamplifier (which was operated uncooled at each temperature) influenced the parallel white noise, as shown in equation 1 [22, 23, 24]. The capacitances of the detector and input JFET of the preamplifier influence the series white noise and 1/*f* noise, as shown in equations 2 and 3 [22, 23, 24]. Parallel white noise and series white noise are, respectively, directly and inversely proportional to the shaping time; whilst 1/*f* noise and dielectric noise are independent of shaping time [22, 23].

$$ENC_{wp} = \frac{1}{q}\sqrt{\frac{A_3}{2}2q(I_D + I_{JFET})\tau} \quad (1)$$

$$ENC_{ws} = \frac{B}{q}\sqrt{\frac{A_1}{2}4kT\frac{\gamma}{g_m}(C_D + C_{JFET})^2\frac{1}{\tau}} \quad (2)$$

$$ENC_{1/f} = \frac{1}{q}\sqrt{A_2\pi\gamma 4kT\frac{f_c}{g_m}(C_D + C_{JFET})^2} \quad (3)$$

where A_1, A_2 and A_3 are 1.85, 1.8, and 1.85, respectively [24]; I_D the experimentally measured packaged device leakage current at different temperatures, I_{JFET} the JFET leakage current at different temperatures (at 20 °C the leakage current of the JFET was 1 pA); C_D the experimentally measured packaged device capacitance at different temperatures, C_{JFET} the JFET capacitance (assumed to be 2 pF at all the temperatures studied), g_m the JFET transconductance (assumed to be 6 mS at the operating condition of the JFET), γ the product of the noise resistance and the transconductance of the JFET (0.85), B the induced gate current correction (0.8)[23], f_c the corner frequency of the JFET (assumed to be 1000 Hz at the operating condition of the JFET) [25].

The obtained parallel white noise, series white noise (adjusted for induced gate current noise [22, 23, 24], and 1/*f* noise, as well as the measured equivalent noise charge, at shaping times of (a) 0.5 μs, (b) 1 μs, and (c) 10 μs, with the $In_{0.5}Ga_{0.5}P$ photodiode reverse biased at 5 V, are shown in Figure 7. In Figure 7 the measured equivalent noise charge was calculated using the value of the $In_{0.5}Ga_{0.5}P$ electron-hole pair creation energy as determined at each temperature in section "3.3. Fano-limited energy resolution and electron-hole pair creation energy".

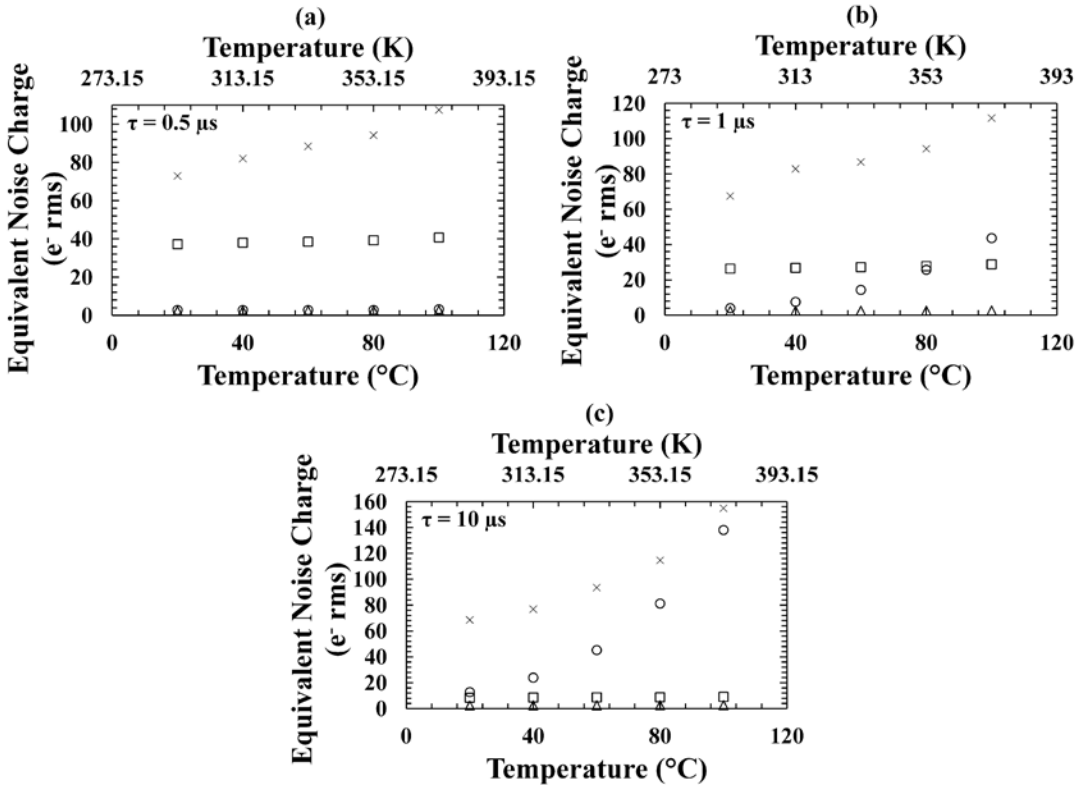

Figure 7. Equivalent noise charge as a function of temperature at shaping time of (a) 0.5 μs, (b) 1 μs, and (c) 10 μs, when the $In_{0.5}Ga_{0.5}P$ photodiode was reverse biased at 5 V. The graphs show the contributions of the parallel white noise (empty circles), the series white noise (empty squares) and the 1/*f* noise (empty triangles), as well as the measured equivalent noise charge (crosses).

The high parallel white noise observed at increased temperatures and at increased shaping times is not due to the high leakage current of the $In_{0.5}Ga_{0.5}P$ detector, but instead due to the higher current of the uncooled Si input JFET of the preamplifier [22].

The FWHM of the 5.9 keV peak as a function of shaping time, reported in Figure 6, shows that at 100 °C the noise was leakage current limited, as expected when combining in quadrature the parallel white noise and the series white noise of Figure 7. Therefore, the shortest shaping time (0.5 μs) gave the best energy resolution. The noise at 20 °C was not leakage current limited, as suggested by the FWHM of the 5.9 keV peak as a function of shaping time (Figure 6). Thus, a long shaping time, 6 μs, resulted in the best energy resolution.

The temperature dependence of the residual noise is shown in Figure 8. At each shaping time, the residual noise was estimated by subtracting in quadrature the known noise components from the measured ENC. In Figure 8a, the residual noise dependence on

the temperature at all the six studied shaping times was reported. In Figure 8b, the mean of the residual noises among the six shaping times (at each point the root mean squared error was associated) as a function of temperature is shown. The measured FWHM was converted into ENC using the values of the electron-hole pair creation energies at each temperature as determined in section "3.3. Fano-limited energy resolution and electron-hole pair creation energy".

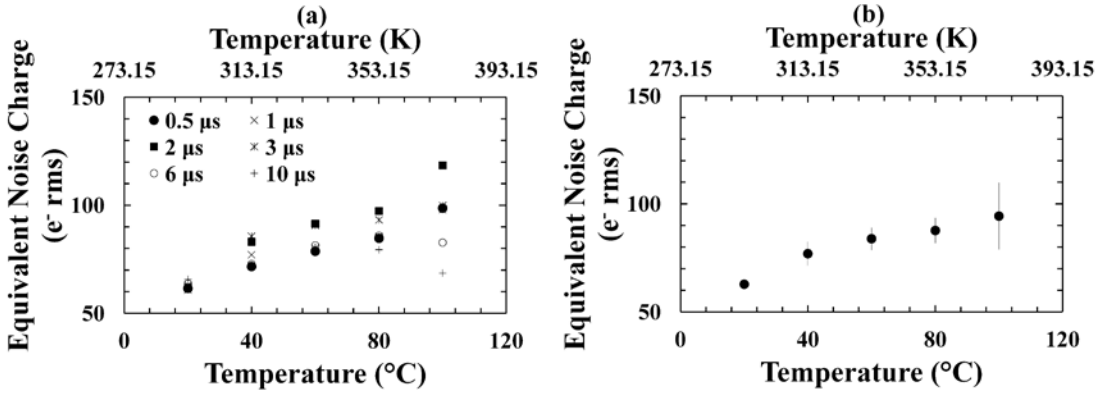

Figure 8. (a) Equivalent noise charge of the residual noise at 5.9 keV at each shaping time studied as a function of temperature, when the $In_{0.5}Ga_{0.5}P$ photodiode was reverse biased at 5 V. (b) Mean of the equivalent noise charge of the residual noise at 5.9 keV among the six shaping times as a function of temperature (at each point the root mean squared error was associated), when the $In_{0.5}Ga_{0.5}P$ photodiode was reverse biased at 5 V.

In the temperature range 100 °C to 20 °C, the residual noise contribution at 5.9 keV linearly decreased with decreasing temperature: at 100 °C a value of 94 e^- rms ± 15 e^- rms was calculated; whilst at 20 °C a value of 63 e^- rms ± 2 e^- rms was determined.

The $In_{0.5}Ga_{0.5}P$ spectrometer allowed high temperature operation (up to the maximum investigated, 100 °C). It presented better FWHM than was achieved using $Al_{0.52}In_{0.48}P$ [5] and $Al_{0.8}Ga_{0.2}As$ [3] spectrometers, but not as good as has been demonstrated using SiC detectors with lower noise readout electronics [4], at the same temperatures. It should also be noted that the use of ultra-low-noise readout electronics, such as those reported in Ref. [26] would likely improve the energy resolution achieved.

The ability to work at such high (100 °C) temperatures together with their greater X-ray attenuation coefficients makes $In_{0.5}Ga_{0.5}P$ spectrometers preferred over recently reported GaAs spectrometers which have a maximum operating temperature of 60 °C [2]. However, at more modest temperatures (e.g. 60 °C) the previously reported GaAs

spectrometer had a better FWHM at 5.9 keV (840 eV) than the $In_{0.5}Ga_{0.5}P$ spectrometer (1.02 keV). The presently reported $In_{0.5}Ga_{0.5}P$ X-ray spectrometer also performed better at 100 °C than the previously reported $Al_{0.52}In_{0.48}P$ X-ray spectrometer. The FWHM at 5.9 keV for the $In_{0.5}Ga_{0.5}P$ device was 1.27 keV at 100 °C c.f. 1.57 keV for the $Al_{0.52}In_{0.48}P$ device using similar device readout electronics. $In_{0.5}Ga_{0.5}P$ also has larger linear attenuation coefficients than $Al_{0.52}In_{0.48}P$.

Since the readout electronics used to characterise these materials have been broadly comparable, the difference in obtained FWHM for these materials (GaAs, AlInP, InGaP) can be explained considering their different electron-hole pair creation energies and the noise contributions of the readout electronics at high temperature (see section "3.3 Fano-limited energy resolution and electron-hole pair creation energy"). A total noise at the input of the preamplifier of 86 e^- rms, for example, corresponds to 840 eV in GaAs, to 1.00 keV in $In_{0.5}Ga_{0.5}P$ and to 1.08 keV in $Al_{0.52}In_{0.48}P$. The observed FWHM of 1.02 keV at 5.9 keV at 60 °C for the $In_{0.5}Ga_{0.5}P$ spectrometer was very close to the expected value. Therefore, the total noise in e^- rms was similar in the GaAs and $In_{0.5}Ga_{0.5}P$ spectrometers, since the preamplifier was limited by noises other than the detector leakage current at these temperatures.

However, the energy resolution achieved with the very best SiC X-ray detectors coupled to much lower noise readout electronics [4] is superior to that obtained with $In_{0.5}Ga_{0.5}P$ and our preamplifier electronics. A SiC detector with FWHM of 233 eV at 5.9 keV has been reported at 100 °C [4]. It would be interesting to characterise the $In_{0.5}Ga_{0.5}P$ detectors with the same ultra-low noise electronics used for the SiC detectors to establish a better comparison between the materials. It should also be noted that the X-ray attenuation coefficients of $In_{0.5}Ga_{0.5}P$ are much greater than those for SiC. Thus, even if the ultimately achievable energy resolution with $In_{0.5}Ga_{0.5}P$ is more modest than SiC, $In_{0.5}Ga_{0.5}P$ may still be preferred for low-flux, high-energy applications.

3.3 Fano-limited energy resolution and electron-hole pair creation energy

The Fano-limited energy resolution is related to the charge creation process at the absorption of an X-ray photon, and is the statistically limited energy resolution of a

non-avalanche X-ray photodiode spectrometer [27]. The Fano-limited energy resolution (FWHM in eV) can be calculated using equation 4:

$$FWHM = 2.35\varepsilon\sqrt{\frac{FE}{\varepsilon}} \quad (4)$$

where ε is the semiconductor electron-hole pair creation energy, F is the Fano factor, and E is the X-ray photon's energy. Different semiconductors have different Fano limited energy resolutions at the same X-ray photon's energy. This is because the Fano limited energy resolution at each energy is dependent on physical material properties (average electron-hole pair creation energy and Fano factor).

For the room temperature (20 °C) measurements of the electron-hole pair creation energy, a method similar to that reported by other researchers [28, 29, 30, 31] was used. The charge created by the absorption of X-rays from the ^{55}Fe radioisotope X-ray source in the $In_{0.5}Ga_{0.5}P$ photodiode was measured relative to that created in a reference 200 μm GaAs mesa photodiode. The structure of the GaAs device is summarised in TABLE 3. The $In_{0.5}Ga_{0.5}P$ and GaAs detectors were connected in parallel to the custom-made low-noise charge-sensitive preamplifier.

TABLE 3. Layer details of the GaAs photodiode.

Layer	**Material**	**Thickness (μm)**	**Dopant**	**Dopant Type**	**Doping density (cm^{-3})**
1	Ti	0.02			
2	Au	0.2			
3	GaAs	0.5	Be	p^+	2×10^{18}
4	GaAs	10	undoped		$<10^{15}$
5	GaAs	1	Si	n^+	2×10^{18}
6	Substrate n^+ GaAs				
7	InGe	0.02			
8	Au	0.2			

The $In_{0.5}Ga_{0.5}P$ and the GaAs photodetectors were both independently reverse biased at 10 V. Spectra were accumulated with the ^{55}Fe radioisotope X-ray source illuminating the $In_{0.5}Ga_{0.5}P$ device and the GaAs device separately, in turn. Gaussians were fitted to the detected Mn Kα (5.9 keV) and Mn Kβ (6.49 keV) peaks of the accumulated

spectra; the ^{55}Fe X-ray spectra accumulated and the fitted 5.9 keV peaks for the $In_{0.5}Ga_{0.5}P$ detector and the GaAs reference photodetector are shown in Figure 9.

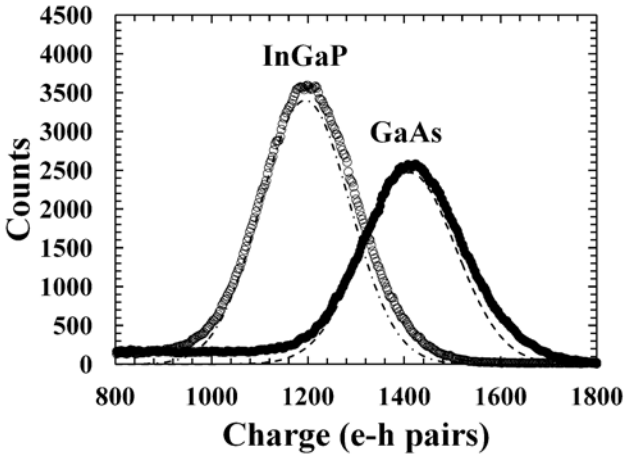

Figure 9. ^{55}Fe X-ray spectra accumulated at 10 V reverse bias using the $In_{0.5}Ga_{0.5}P$ device (empty circles) and the GaAs reference photodetector (filled circles) under the illumination of ^{55}Fe radioisotope X-ray source. Also shown are the fitted 5.9 keV lines for the $In_{0.5}Ga_{0.5}P$ device (dashed-dot line) and the GaAs reference photodetector (dashed line). For clarity, the fitted 6.49 keV Mn Kβ peaks are not shown but were included appropriately in the fitting.

The quantity of charge corresponding to each MCA channel was calculated using the position of the zero noise energy peak of the preamplifier and the 5.9 keV peak detected by the GaAs reference photodiode. In this calculation, the GaAs electron-hole pair creation energy, 4.184 eV ± 0.025 eV, [28] was also used. The $In_{0.5}Ga_{0.5}P$ electron-hole pair creation energy (ε_{InGaP}) was then determined using equation 5:

$$\varepsilon_{InGaP} = \varepsilon_{GaAs}\left(\frac{N_{GaAs}}{N_{InGaP}}\right) \quad (5)$$

where ε_{GaAs} is the electron-hole pair creation energy in GaAs, N_{GaAs} and N_{InGaP} are the number of charges created in the GaAs reference detector and $In_{0.5}Ga_{0.5}P$ detector, respectively. An experimental value of 4.94 eV ± 0.06 eV was measured for ε_{InGaP} at room temperature (20 °C). To examine the effect of operating the $In_{0.5}Ga_{0.5}P$ detector at higher reverse biases, the reverse bias was increased to 15 V, and the experiment repeated. An electron-hole pair creation energy of 4.90 eV ± 0.04 eV was measured in this instance. The similarity of the values further confirms that charge trapping was negligible. If charge trapping was significant, a substantial reduction in apparent

electron-hole pair creation energy would have been observed at higher reverse bias as a consequence of the improved charge transport at higher electric field.

The dependence of the $In_{0.5}Ga_{0.5}P$ electron-hole pair creation energy upon temperature was studied across the temperature range 100 °C to 20 °C. For this set of measurements, the $In_{0.5}Ga_{0.5}P$ detector was individually connected to the custom-made low-noise charge-sensitive preamplifier (i.e. without the GaAs reference detector) and illuminated by the ^{55}Fe radioisotope X-ray source. The change in conversion factor of the preamplifier itself with temperature was measured across the temperature range by connecting a stabilized pulse generator (Berkeley Nucleonics Corporation model BH-1) to the test signal input of the preamplifier. The change in position of the centroid of the pulse generator peak allowed the change in performance of the preamplifier with temperature to be untangled from the change in electron-hole pair creation energy of the photodiode. The change in position of the centroid of the pulse generator peak was appropriately corrected for the change in the test capacitance with temperature [32]. Spectra were collected and Gaussians were fitted to the photopeak and the peak from the pulse generator in order to determine the positions of their centroids with respect to the zero noise peak. The charge created in the $In_{0.5}Ga_{0.5}P$ photodiode by the X-ray photons was related to the relative change in position of the photopeak on the MCA's charge scale. The latter was corrected for the preamplifier's change in conversion factor with temperature (determined from the pulser peak) [31, 33]. The different quantities of charge created at different temperatures was caused by the change in the $In_{0.5}Ga_{0.5}P$ electron-hole pair creation energy (ε_{InGaP}). At each temperature, the absolute value of ε_{InGaP} was then computed using the previously determined room temperature ε_{InGaP}. The apparent $In_{0.5}Ga_{0.5}P$ electron-hole pair creation energy as a function of temperature is reported in Figure 10. The uncertainties associated with the electron-hole pair creation energy values were obtained by propagating the uncertainty in the electron-hole pair creation energy at room temperature and the uncertainty in the relative change in the conversion factors. The uncertainty in the electron-hole pair creation energy at room temperature (± 0.06 eV) was an order of magnitude greater than the uncertainties in the relative change in the conversion factors (± 0.005 eV); therefore, the former mainly affected the uncertainties in the electron-hole pair creation energy at different temperatures. A similar experimental setup was used by other

researchers to measure the electron-hole pair creation energy in other materials [31, 33].

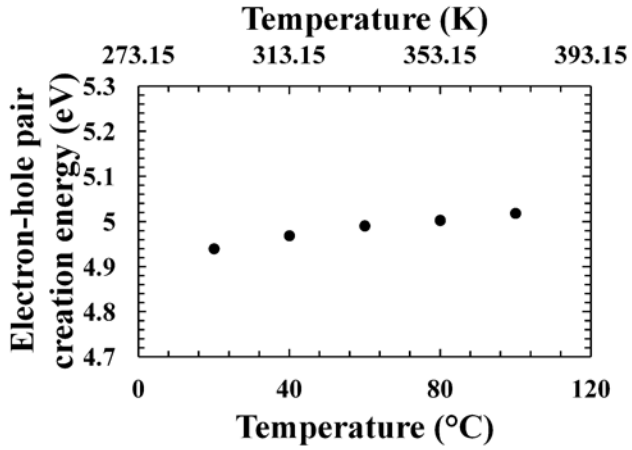

Figure 10. Temperature dependence of the energy consumed to produce an electron-hole pair in $In_{0.5}Ga_{0.5}P$.

An apparent slight trend suggesting that the $In_{0.5}Ga_{0.5}P$ electron-hole pair creation energy increased with increasing temperature was found: at 100 °C, ε_{InGaP} = 5.02 eV ± 0.07 eV, whereas at 20 °C ε_{InGaP} = 4.94 eV ± 0.06 eV. However, the data points were all within the uncertainties of each other for the temperature range investigated. If the trend (greater average electron-hole pair creation energy at higher temperatures) was real, the results would be surprising. It is conventionally considered that the average electron-hole pair creation energy decreases linearly as the temperature increases [28, 31, 33, 34, 35]. Such a decrease can be understood considering the dependence of the electron-hole pair creation energy on the material bandgap energy. According to Klein [36], the empirical relationship between the electron-hole pair creation energy and the bandgap energy in a semiconductor is linear. Since the bandgap decreases at increased temperatures, a similar behaviour is expected for the electron-hole pair creation energy, due at least in part to the change in bandgap. Theoretical Monte Carlo calculations conducted by Fraser et al. [34] for silicon predicted the decrease of the Si electron-hole pair creation energy as a function of temperature.

The expected Fano limited energy resolution (FWHM) at 5.9 keV of X-ray detectors made from $In_{0.5}Ga_{0.5}P$ was estimated using equation 4 and the determined values for the electron-hole pair creation energy. The Fano factor for $In_{0.5}Ga_{0.5}P$ has not yet been

514 measured, but assuming a Fano factor of 0.12 (as for GaAs [37]), the Fano limited
515 energy resolution would be expected to be 139 eV at 5.9 keV at 20 °C. If the Fano
516 factor was 0.099 (as for CdZnTe [38]) a Fano limited energy resolution of 127 eV at
517 5.9 keV would be expected at 20 °C. Negligible changes over the 20 °C to 100 °C
518 temperature range were observed.
519
520 The electron-hole pair creation energy at 27 °C (300 K), which was interpolated from
521 the experimental measurements at 20 °C (293 K) and 40 °C (313 K), equalled 4.95 eV
522 ± 0.07 eV. This is in agreement with the value predicted for $In_{0.5}Ga_{0.5}P$ (4.83 eV ±
523 0.21 eV) by the empirical Bertuccio-Maiocchi-Barnett (BMB) relationship [31]. Figure
524 11 shows the average electron-hole pair creation energy for Ge, Si, GaAs, $Al_{0.2}Ga_{0.8}As$,
525 $Al_{0.8}Ga_{0.2}As$, $Al_{0.52}In_{0.48}P$ [39], and $In_{0.5}Ga_{0.5}P$, and as a function of their respective
526 bandgap energies, at a temperature of 300 K.

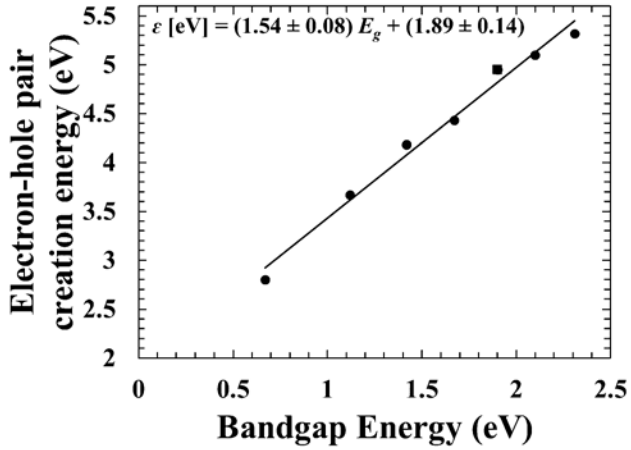

527
528 Figure 11. Electron-hole pair creation energy for Ge, Si, GaAs, $Al_{0.2}Ga_{0.8}As$,
529 $Al_{0.8}Ga_{0.2}As$, and $Al_{0.52}In_{0.48}P$ (filled circles), and $In_{0.5}Ga_{0.5}P$ (filled square), as a
530 function of their bandgap energy at 300 K. The equation shown for the relationship has
531 been refined using the new data for $In_{0.5}Ga_{0.5}P$.
532
533 A linear least squares fit of the data showed that the previously reported BMB
534 dependence between electron-hole pair creation energy and bandgap energy can be
535 refined using the new data for $In_{0.5}Ga_{0.5}P$. The new relation is $\varepsilon = AE_g + B$ with A =
536 (1.54 ± 0.08) and B = 1.89 eV ± 0.14 eV. Using this relationship, the ε_{InGaP} would be
537 expected to be 4.82 eV ± 0.3 eV.
538
539 As is the case for $Al_{0.8}Ga_{0.2}As$ [30, 33] and $Al_{0.2}Ga_{0.8}As$ [31], the electron-hole pair
540 creation energy value reported here at 300 K for $In_{0.5}Ga_{0.5}P$ does not lie either on the

main or secondary Klein function branches [1, 36]. If $In_{0.5}Ga_{0.5}P$ was on the main Klein function branch, the expected ε_{InGaP} would be 6.17 eV, which is substantially higher than that found here (4.95 eV ± 0.03 eV). If it was on the secondary Klein function branch, the expected ε_{InGaP} would be 4.07 eV, which is substantially lower than the obtained value. This lends further weight to the view that the Klein relationship is incomplete [31].

4. CONCLUSIONS

For the first time an X-ray spectrometer with an InGaP detector was demonstrated across the temperature range 100 °C to 20 °C. The spectrometer was characterised at different shaping times and detector reverse biases. The best energy resolution (smallest FWHM) at 5.9 keV was 1.27 keV at 100 °C using a shaping time of 0.5 μs, this improved to 770 eV at 20 °C (using a shaping time of 6 μs), when the $In_{0.5}Ga_{0.5}P$ detector was reverse biased at 5 V. An improvement in energy resolution (as quantified by the FWHM at 5.9 keV) was observed when increasing the applied reverse bias from 0 V to 5 V. The better results obtained at 5 V can be explained considering the improved charge collection in the greater electric field strength. Similar FWHM to that measured at 5 V were observed at 10 V and 15 V, suggesting that charge trapping noise at 5 V and above was negligible. System noise analysis showed that the observed FWHM were higher than the likely statistically limited energy resolution (i.e. the Fano-limited energy resolution). The parallel white noise, series white noise, $1/f$ noise, and residual noise were calculated. The higher parallel white noise observed at increased temperatures was caused by the Si input JFET of the preamplifier rather than the photodetector. At 100 °C and at 0.5 μs, for example, parallel white noises of 30.8 e^- rms for the Si JFET and 2.8 e^- rms for the $In_{0.5}Ga_{0.5}P$ device were found when the diode was reversed bias at 15 V. A dedicated experiment was conducted to measure the $In_{0.5}Ga_{0.5}P$ average electron-hole pair creation energy (ε_{InGaP}) in the temperature range 100 °C to 20 °C. ε_{InGaP} was found to be 4.94 eV ± 0.06 eV at 20 °C and 5.02 eV ± 0.07 eV at 100 °C.

ACKNOWLEDGMENTS

This work was supported by STFC grants ST/M004635/1 and ST/P001815/1 (University of Sussex, A. M. B., PI). A. M. B. acknowledges funding from the

Leverhulme Trust in the form of a 2016 Philip Leverhulme Prize. The authors are grateful to B. Harrison for growth of the GaAs structure, and R. J. Airey and S. Kumar for device fabrication and processing at the EPSRC National Epitaxy Facility for material growth and device fabrication.

REFERENCES

[1]A. Owens, A. Peacock, Nucl. Instrum. Meth. Phys. Res. A 531 (2004) 18.

[2]G. Lioliou, X. Meng, J. S. Ng, A. M. Barnett, Nucl. Instrum. Meth. Phys. Res., Sect. A 813 (2016) 1.

[3]A. M. Barnett, J. E. Lees, D. J. Bassford, J. S. Ng, C. H. Tan, N. Babazadeh, R. B. Gomes, Nucl. Instrum. Meth. Phys. Res., Sect. A 654 (2011) 336.

[4]G. Bertuccio, S. Caccia, D. Puglisi, D. Macera, Nucl. Instrum. Meth. Phys. Res., Sect. A 652 (2010) 193.

[5]S. Butera, T. Gohil, G. Lioliou, A. B. Krysa, A. M. Barnett, J. Appl. Phys 120 (2016) 174503.

[6]M. R. Squillante, G. Entine Nucl. Instrum. Meth. Phys. Res. A 380 (1996) 160.

[7]S. U. Egarievwe, K. T. Chen, A. Burger, R. B. James, C. M. Lisse, J. X-ray Sci. Technol. 6 (1996) 309.

[8]A. Zappettini, D. Macera, G. Benassi, N. Zambelli, D. Calestani, M. Ahangarianabhari, Y. Shi, G. Rotondo, B. Garavelli, P. Pozzi, G. Bertuccio, IEEE Nuclear Science Symposium and Medical Imaging Conference (NSS/MIC) (Seattle, WA, 8-15 November 2014).

[9]L. Abbene, G. Gerardi, G. Raso, F. Principato, N. Zambelli, G. Benassi, M. Bettelli, A. Zappettini, J. Synchrotron Rad. 24 (2017) 429.

[10]S. Butera, G. Lioliou, A. B. Krysa, A. M. Barnett, Sci. Rep. 7 (2017) 10206.

[11]A. Owens, Compound semiconductor radiation detectors, CRC Press, Boca Raton, 2012.

[12]A. Owens, S. Andersson, R. Den Hartog, F. Quarati, A. Webb, E. Welter, Nucl. Instr. and Meth. A 581 (2007) 709.

[13]A. Owens, M. Bavdaz, V. Gostilo, D. Gryaznov, A. Loupilov, A. Peacock, H. Sipila, Nucl. Instr. and Meth. A 487 (2002) 435.

[14]A. Owens, A. Peacock, M. Bavdaz, G. Brammertz, F. Dubecky, V. Gostilo, D. Gryaznov, N. Haack, M. Krumrey, A. Loupilov, Nucl. Instr. and Meth. A 491 (2002) 444.

[15] J. H. Hubbell, Int. J. Appl. Radiat. Is. 33 (1982) 1269.

[16]R. Jenkins, R. W. Gould, D. Gedcke, Quantitative X-ray Spectrometry, Second Ed., CRC Press, New York, 1995.

[17]S. Minagawa, M. Kondow, Electron. Lett. 25 (1989) 758.

[18]Keithley Instruments, Inc, *Model 6487 Picoammeter/Voltage Source Manual*, 6487-901-01 Rev B, Cleveland, 2011.

[19]Hewlett Packard, *Model HP4275A Multi-Frequency LCR Meter Manual*, 04275-90004, Tokyo, 1990.

[20]G. Bertuccio, P. Rehak, D. Xi, Nucl. Instrum. Meth. Phys. Res. B 326 (1993) 71.

[21]U. Shotzig, Applied Radiation and Isotopes 53 (2000) 469.

[22]G. Lioliou, A. M. Barnett, Nucl. Instrum. Meth. Phys. Res. A 801 (2015) 63.

[23]G. A. Bertuccio, A. Pullia, G. De Geronimo, Nucl. Instrum. Meth. Phys. Res. A 380 (1996) 301.

[24]E. Gatti, P. F. Manfredi, M. Sampietro, V. Speziali, Nucl. Instrum. Meth. Phys. Res., A 297 (1990) 467.

[25]Vishay Siliconix, *2N4416/2N4416A/SST4416 N-Channel JFETs Data Sheet*, 70242 S-50147 Rev. H, Selb, 2005.

[26]G. Bertuccio, D. Macera, C. Graziani, M. Ahangarianaghari, IEEE Nuclear Science Symposium and Medical Imaging Conference (NSS/MIC) (Seattle, WA, 8-15 November 2014)

[27]G. W. Fraser, X-ray Detectors in Astronomy, Cambridge University Press, Cambridge, 1989.

[28]G. Bertuccio, D. Maiocchi, J. Appl. Phys. 92 (2002) 1248.

[29]G. Bertuccio, R. Casiraghi, IEEE Trans. Nucl. Sci. 50 (2003) 175.

[30]A. M. Barnett, J. E. Lees, D. J. Bassford, J. S. Ng, J. Inst. 7 (2012) P06016.

[31]M. D. C. Whitaker, S. Butera, G. Lioliou, A.M. Barnett, J. Appl.Phys. 122 (2017) 034501.

[32]K. Lamkaouchi, A. Balana, G. Delbos, W. J. Ellison, Meas. Sci. Technol. 14 (2003) 444.

[33]A. M. Barnett, J. E. Lees, D. J. Bassford, Appl. Phys. Lett. 102 (2013) 181119.

[34]G. W. Fraser, A. F. Abbey, A. Holland, K. McCarthy, A. Owens, A. Wells, Nucl. Instrum. Meth. Phys. Res., A 350 (1994) 368.

[35]M. N. Mazziotta, Nucl. Instrum. Meth. Phys. Res., A 584 (2008) 436.

[36]C. A. Klein, J. Appl. Phys. 39 (1968) 2029.

[37]G. Bertuccio, A. Pullia, J. Lauter, A. Forster, H. Luth, IEEE Trans. Nucl. Sci. 44 (1997) 1.

[38]A. Owens, M. Bavdaz, H. Andersson, T. Gagliardi, M. Krumrey, S. Nenonen, A. Peacock, I. Taylor, L. Tröger. Nucl. Instrum. Meth. Phys. Res., A. 484 (2002) 242.

[39]S. Butera, G. Lioliou, A. B. Krysa, A. M. Barnett. Nucl. Instrum. Meth. Phys. Res., A. 879 (2017) 64.